

PHYSICAL REVIEW B

CONDENSED MATTER

THIRD SERIES, VOLUME 44, NUMBER 2

1 JULY 1991-II

Behavior of point defects in a model crystal near melting

Charles H. Martin and Sherwin J. Singer
Department of Chemistry, Columbus, Ohio 43210
(Received 26 December 1990)

Premelting near point defects has on many occasions been proposed as a melting mechanism, most recently to interpret x-ray-absorption fine-structure and Mössbauer results for impurities in a lead crystal. We studied the behavior of point defects in a model soft-core crystal. Because of its small density change upon melting, the soft-core crystal should be better than hard-core models in accommodating a liquid droplet that has a larger specific volume than the solid. We have failed to observe premelting near isolated point defects (vacancies, polyvacancies, and impurities) in an inverse-6 soft-core model. When vacancies and polyvacancies were deliberately surrounded by a liquidlike region in numerical simulations, this region spontaneously ordered under all conditions where the solid was thermodynamically stable. This eliminates the possibility that a kinetic barrier prevented the observation of premelting. When impurities of sufficiently great size mismatch from the bulk particles are introduced into the model, the impurities diffuse as interstitials near the melting point, but isolated impurities do not produce unusually disordered regions near melting.

I. INTRODUCTION

Recent experimental evidence suggests that melting is initiated near point defects in crystals.¹⁻³ In this work we examine the degree to which this phenomena occurs in computer simulations of a model crystal. X-ray-absorption fine-structure (XAFS) spectra of dilute Hg impurities in a Pb host¹ show the amplitude of vibration of the impurity increasing linearly with temperature at low temperature, as expected in the harmonic limit, but unexpectedly saturating at 400 K, 180° below the bulk lead melting temperature of 580 K. Also, the Hg coordination number, which is determined indirectly from the spectra, drops from 12 at 400 K to 8 at the melting point. Stern and Zhang explain the data in terms of a liquid pocket which forms about the impurity, the pocket growing in size as temperature rises.¹

The formation of liquid regions around *non-equilibrium* defects below bulk melting has been documented for free surfaces and grain boundaries,^{4,5} and has been suggested to occur near other nonequilibrium defects.^{6,7} Point defects are *equilibrium* defects, however, and therefore the possibility of point-defect premelting is both novel and of fundamental significance to understanding the mechanism of melting.⁸⁻¹⁰ Stern and Zhang argue that point-defect initiated melting should lower the bulk melting temperature in the thermodynamic limit, dominating over melting initiated by nonequilibrium defects. Supporting the evidence for premelted regions forming about impurities, Shechter *et al.* report that a

Mössbauer experiment on 1% concentrations of Sn in a Pb host shows an anomalous decrease in the integrated resonance intensity at a critical temperature, $T_c = 150$ K, well below bulk melting.² They also observe no line broadening, which indicates the impurity does not simply diffuse. They explain these data by postulating the existence a high-temperature "premelted bubble," a region of large entropy density, comprised of about 50 particles with amplitudes of vibration comparable to liquid particles. Pokorny and Grimvall report an unexpected increase in the resistivity of pure lead beginning 60 K below the bulk melting temperature.³ Their data is interpreted in terms of the appearance of a high entropy, liquidlike defect near melting. The idea of locally liquidlike disorder near point defects in the solid phase has been suggested from time to time in connection with vacancy motion and anomalous behavior of thermodynamic quantities near melting.¹¹⁻¹³

Here we describe detailed observations of vacancies and impurities in a computer simulation of a model system, a face-centered-cubic (fcc) crystal of "soft" spheres that interact via an r^{-6} repulsive potential. Briefly, we first attempted to initiate melting at vacancies in systems with both hard-sphere and soft-core r^{-n} potentials. After not observing premelted regions, we constructed a novel simulation technique to introduce liquid droplets into a simulated crystal. This procedure was applied to the soft-core model which, in Sec. II, we argue should be most likely to exhibit point-defect premelting. We found that translationally disordered pockets surrounding va-

cancies were actually *unstable* inside our model crystals at or above the bulk melting point. Finally, we modeled an impurity by substituting one smaller particle into the simulated crystal. The behavior of the impurity suggests alternative interpretations of the XAFS and Mössbauer experiments. We emphasize, however, that our model (chosen for reasons discussed below) is very simple, and that very different behavior might result from potentials more faithful to the actual experimental systems.

The mechanism of crystal melting has long been a controversial subject.^{14,15} It does not make sense to search for just one melting mechanism that is correct for all situations. Surface properties, the presence or absence of nonequilibrium defects, and the degree of superheating are all known to affect the melting process. Surface effects on melting have been demonstrated by observing small systems. Superheating of small particles in a rigid matrix shows that free surfaces facilitate melting. Saka *et al.* heated small indium particles embedded in an aluminum matrix.¹⁶ For In particles with radii < 15 nm, the melting temperatures were between 170 and 200 °C, at least 24 °C above the In bulk melting temperature of 156 °C. Furthermore, the melting temperatures increased with smaller radii. This contrasts with the behavior of free particles, which melt more easily when the radii are smaller.¹⁷ Saka and co-workers explain the increased indium particle melting temperature in terms of the interfacial free-energy cost to form the liquid-solid interface.

Experiments and computer simulations exhibit premelting near grain boundaries (GB) and crystal-vapor (CV) surfaces. In a proton scattering experiment, Frenken and Van der Veen observed backscattering spectra from the surface of a Pb specimen.⁴ They proposed that a liquid layer three planes deep formed at 40 K below the bulk melting temperature, and that this layer became deeper as temperature increased. In computational studies of a crystal composed of particles interacting with the Lennard-Jones (LJ) potential, Broughton and Gilmer observed melted regions below the bulk melting transition at crystal-vapor^{18,5} and grain-boundary^{19,5} surfaces.⁵ As temperature increased, the melted regions grew, engulfing the entire crystal at the bulk transition. These and other studies^{20–24} make evident the role surfaces play in melting of crystals. Furthermore, they demonstrate that molecular-dynamics (MD) simulations of rather simple model potentials can reproduce some of the general features of melting. Recent simulations of silicon²⁵ and copper²⁶ using many-body potentials illustrate how one must be cautious in drawing general conclusions based upon study of just one potential model. No GB premelting was observed in the many-body potential simulations, in contrast to earlier simulations using pair potentials.

Further experiments on nonequilibrium defects in various systems indicate defects other than surfaces may also initiate melting and/or support premelted regions. Bartis interpreted the steep rise of the self-diffusion of molten pivalic acid near its melting point as the consequence of molten regions along dislocations.⁷ Bartis also invokes premelting about dislocations to explain the thermal expansivity of benzene and butane-1,4-diol near melting.⁶

The degree of superheating also influences the initia-

tion of melting. Cotterill, Jensen, and Kristensen, studying the dynamics of the melting transition in a rather highly superheated Lennard-Jones crystal, found melting occurred through the spontaneous generation of dislocation loops.^{27,28} It is possible, however, that melting of a highly superheated crystal may proceed by an entirely different mechanism than in a system much closer to equilibrium.

To our knowledge, the only previous attempt to induce point-defect premelting in numerical simulations is the work of Lutsko *et al.* in which a copper crystal was simulated using an embedded-atom-method potential.²⁶ No evidence of premelting was observed after 1, 5, or 13 vacancies were introduced in what was originally a 108-particle sample. Our results confirm the absence of vacancy-induced premelting for a different potential model. Besides furnishing information on a new system, we also take care to eliminate kinetic effects as an explanation for not observing vacancy-induced premelting in numerical simulations. The Monte Carlo technique described in Sec. III introduces a liquidlike region into a portion of the crystal lattice, and it also confines polyvacancies to that portion of the lattice. In addition to vacancies and polyvacancies, the behavior of impurities near melting is investigated in this work.

The success of computer simulations in elucidating the role of surfaces and defects in melting phenomena motivates our investigation of point-defect premelting in model systems. In Sec. II we explain why a soft-core system was chosen for detailed studies. Our evidence for the absence of premelting near vacancies (including polyvacancies) is presented in Sec. III. The behavior of impurities near the bulk melting point is described in Sec. IV. General discussion with speculations concerning alternative explanations of the Mössbauer data is given in Sec. V.

II. THE SOFT-CORE MODEL SYSTEM

Here we provide theoretical and experimental motivation for searching for premelting in model crystals governed by the “inverse-6” pair potential, $v(r) = \epsilon(\sigma/r)^{-6}$. Simple, classical pair potentials do reproduce general aspects of melting in computational experiments, hence, we felt such models should reproduce point-defect premelting if, indeed, it is a general feature of melting. For example, systems of particles with either hard-sphere or Lennard-Jones interactions accurately model aspects of rare-gas solids and liquids.²⁹ The family of inverse- n potential systems has been studied as a function of n from the hard-sphere limit ($n \rightarrow \infty$) to $n = 3$, the softest inverse- n potential for which the thermodynamic limit exists in three dimensions.^{30–33} The Lennard-Jones pair potential was used in simulations of crystal-vapor surface and grain-boundary premelting.⁵ Certainly systems of particles interacting with simple pair potentials reproduce many qualitative features of melting and premelting.

The repulsive part of the Lennard-Jones potential is quite steep, which is why hard spheres are a good reference system in a perturbative treatment of the Lennard-

Jones system.²⁴ Even though vacancies have been studied intensively in hard sphere, Lennard-Jones, and similar systems,^{35,36} local disordering near vacancies has never been noted in simulations of these systems.^{37,38} In all cases the relaxation of particles near a vacancy is estimated to be no more than a few percent of a nearest-neighbor distance. Our own experiments with hard spheres showed no evidence of disordering near vacancies, even for a metastable crystal above the thermodynamic melting point. Furthermore, no evidence for premelting is observed in solid Ar or Kr.¹⁰ Therefore, particles with steep repulsive cores do not seem likely to exhibit point-defect premelting.

Particles with a softer repulsive core would be more likely to exhibit point-defect initiated premelting, according to the qualitative argument presented here. Weeks showed that the density increase upon melting for the family of inverse- n systems decreases with decreasing n and approaches zero as n approaches 3 from above.³³ In essence, the smaller density increase upon melting lessens the pressure-volume work needed to create a premelted drop surrounding a vacancy or point defect in a solid. Let us consider factors affecting the free-energy change for creation of a premelted drop surrounding a polyvacancy in which n_{vac} lattice sites are vacant. For simplicity assume that the premelted region is spherical (Fig. 1) with radius R . We will find that the net volume change on premelting of the microscopic droplet is negative when R is less than a certain critical radius R_0 , and positive when R is greater than R_0 . Since we also estimate that R_0 increases as the exponent n decreases, we conclude that small exponent systems would allow larger premelted regions before pressure-volume work considerations render premelting unfavorable.

The equilibrium vacancy concentration is usually small, even near melting, so the volume per particle of the solid v_s is approximately equal to the volume per lattice site. Therefore, N_p , the number of particles involved in the premelting, is related to the radius R of the premelted droplet by

$$(N_p + n_{\text{vac}})v_s = \frac{4\pi R^3}{3}, \quad (1)$$

where n_{vac} would be 1 for an ordinary single-site vacancy. The volume per particle in the hypothetical premelted region is thus crudely estimated to be

$$\frac{4\pi R^3}{3N_p}. \quad (2)$$

Clearly, if the volume per particle of the disordered region was significantly greater than v_l , that of a supercooled liquid at the same temperature and pressure, then premelting would be favored. Alternatively, premelting would not be favored if the volume per particle was less than v_l and there was no room to accommodate expansion upon disordering. Solving for N_p in Eq. (1) and substituting into Eq. (2), we find the volume per particle in the premelted droplet as a function of R to be

$$v_s \left[1 - \frac{n_{\text{vac}} v_s}{\frac{4}{3}\pi R^3} \right]^{-1}. \quad (3)$$

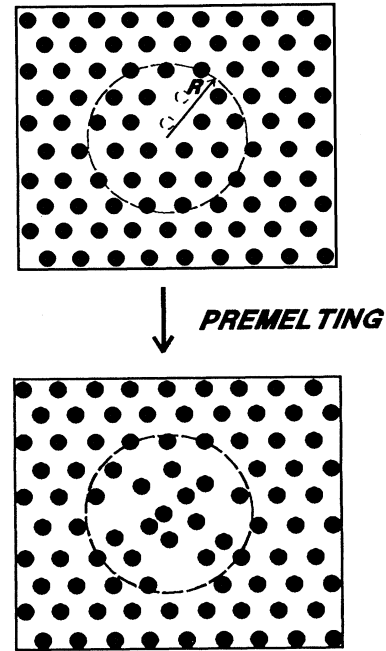


FIG. 1. In this hypothetical premelting event, a spherical region of radius R containing n_{vac} vacancies ($n_{\text{vac}}=2$ is shown in the upper panel) disorders as the bulk melting point is approached. The volume per particle is v_s in the solid. The volume per particle in the spherical premelted region is given in Eq. (3). When the radius of the droplet equals R_0 [Eq. (4)] the volume per particle equals v_l , that of a supercooled liquid under the same thermodynamic conditions as the solid shown above.

For very large droplets the volume per particle must drop to v_s , a very unfavorable situation if the droplet has liquidlike disorder. The volume per particle increases as R decreases. We define R_0 to be the radius at which the volume per particle equals v_l . Equation (3) loses physical meaning for very small R and diverges as R approaches the vacancy radius. It is only for droplets with radii less than R_0 for which pressure-volume considerations favor droplet formation. Even for $R < R_0$, an interfacial free-energy term must also be overcome to allow premelting.

Large R_0 favors premelting, although this is but one of several considerations (among which the solid-liquid interfacial energy of the droplet is probably most important). In general, small density change upon melting leads to large values of R_0 . Thus, we conclude that vacancy premelting, if it occurs, is favored by soft-core potentials, those with the smallest density change upon freezing. When the droplet volume is much larger than $n_{\text{vac}}v_s$, R_0 is approximately given as

$$R_0 \approx \left[\frac{3n_{\text{vac}}v_s^2}{4\pi(v_l - v_s)} \right]^{1/3}, \quad (4)$$

showing how in this crude picture small volume changes and, hence, inverse- n potentials with small n favor large

disordered regions.

A soft inverse- n potential models metal systems better than the hard-core and LJ potentials, hence, we expect it to serve as a better model for elucidating the general features of melting in metal systems. For example, Meyer, Silbert, and Young showed that introducing a finite force at the hard-sphere diameter, hence softening the potential, allowed them to fit the structure factor for lead better than with just a hard-core model.³⁹ Grindley found soft cores with $n=12$ and 15 superior to hard spheres in fitting the compressibility and excess entropy as a function of temperature for liquid Hg.⁴⁰ One should note that lead and mercury were materials used in the experiments which suggested point-defect premelting.¹

Given that hard-sphere and Lennard-Jones systems showed no preliminary evidence of disordering near vacancies, that soft-core systems could accommodate larger premelted regions, and that experimental observations of apparent point-defect premelting occurred in metals, we chose the softest-core potential that was numerically tractable for careful observations of point defects near the bulk melting point. Values of n less than 6 lead to numerical problems associated with truncation of the potential at the boundaries of the simulation cell. Therefore, the $n=6$ inverse power potential was chosen for our studies. It is doubtful that more realistic potentials, even for metals, would contain a softer repulsive core.

Inverse- n potentials are particularly convenient for theoretical modeling. It is well known that the partition function depends upon temperature and density only in the combination $\rho\sigma^3(\beta\epsilon)^{3/n}$ in three dimensions. Therefore, determination of the properties of an inverse- n system along one isotherm or isochore is sufficient to determine the entire temperature-density plane. In the following, we collapse the density and temperature of the inverse- n system into a single reduced density,

$$\rho^* \equiv \rho\sigma^3(\beta\epsilon)^{3/n}. \quad (5)$$

Occasionally it is more intuitive to regard the single parameter that controls the inverse- n system as a reduced temperature,

$$\frac{1}{T^*} \equiv \beta\epsilon(\rho\sigma^3)^{n/3}. \quad (6)$$

At the melting transition, solid at density $\rho^*=2.206$ coexists with liquid at $\rho^*=2.178$.³¹ In all the simulations of inverse-6 systems presented in Secs. III and IV, the lattice structure of the solid was taken to be face-centered cubic. The structure of lead, the bulk material used in XAFS,¹ Mössbauer,² and resistivity³ measurements, is also the close-packed fcc structure. Actually, the inverse-6 model is known to undergo a solid-solid phase transformation to a body-centered-cubic (bcc) lattice.³² It is, however, both convenient and most relevant to experiments to focus solely on the fcc crystal. As in previous work by Hoover *et al.*,³¹ we study the melting of what is not the thermodynamically stable solid phase. Since the likelihood of spontaneous transformation to the bcc structure is negligible, there is nothing ill defined in this procedure.

III. VACANCIES AND POLYVACANCIES NEAR MELTING

Should simple particle size mismatch lead to point-defect premelting, then vacancies and polyvacancies are logical candidates for observing this effect. Vacancies can be viewed as the extreme limit of size mismatch between an impurity and bulk atoms in a crystal. Our results are negative. Vacancy-induced premelting was not observed for inverse-6 soft spheres. The bulk of the work presented in this section describes our efforts to rule out insufficient simulation times as a cause of these negative results. Some of our observations are relevant to point-defect premelting, should it ever be observed in other systems. Based on observation of liquid droplets in an *artificially stabilized* crystal above the bulk melting point, we predict that a finite-sized region surrounding a point defect can fluctuate between ordered and disordered configurations on a time scale much longer than an atomic vibration. This is in complete analogy with molecular-dynamics simulations of finite-sized van der Waals clusters which, in a particular temperature range, exhibit occasional and reversible transitions between solidlike and liquidlike configurations.⁴¹ We cannot rule out that certain potentials may lead to vacancy-induced premelting while the r^{-6} soft spheres studied here failed to exhibit the effect.

Molecular-dynamics simulations of face-centered-cubic crystals interacting via the potential function

$$\epsilon \sum_{i < j} \left[\frac{\sigma}{|\mathbf{r}_i - \mathbf{r}_j|} \right]^6 \quad (7)$$

showed no evidence of liquidlike disorder near single vacancies, or when as many as four vacancies were introduced in the system. The degree of crystalline order was measured in two ways. Firstly, the order parameter

$$\rho_{\mathbf{k}} = \frac{1}{N} \sum_{i=1}^N e^{i\mathbf{k}\cdot\mathbf{r}_i}, \quad (8)$$

the Fourier component of the density at a reciprocal-lattice vector of the fcc lattice [typically $\mathbf{k}=(2\pi/a)(1,1,1)$ in this work], was monitored as a function of time. The behavior of the order parameter as the system is brought through the solid-liquid coexistence region is discussed later in this section. Secondly, a representation of the overall particle density was tracked by making trajectory plots of the type shown in Fig. 2. The particle trajectories shown in Fig. 2 were obtained at a density which lies in the liquid region of the phases diagram. The solid is metastable in the simulation. In spite of the superexpanded state of the solid, periodic translational order is maintained throughout the system, without evidence that a premelted region persists in the neighborhood of a vacancy.

A free-energy barrier might separate the (relatively) unrelaxed crystalline configuration we observed surrounding vacancies, and premelted configurations. In this case, very long simulation times may be required until the crystal explores locally disordered configurations. To ascertain with certainty whether the highly ordered

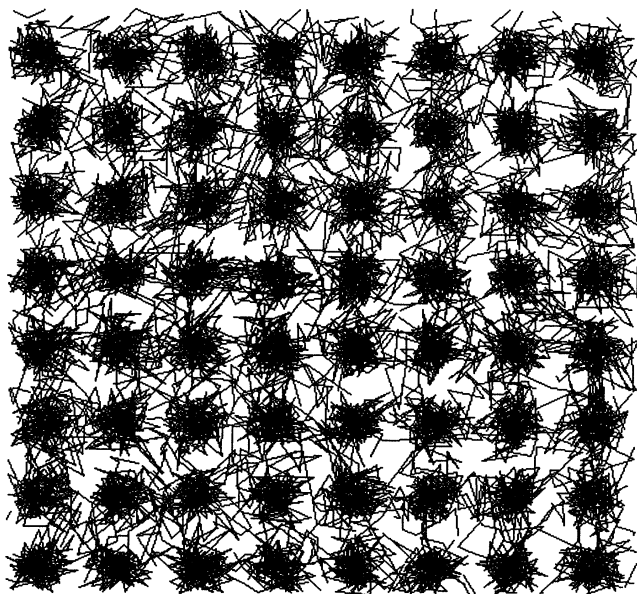


FIG. 2. Trajectory plot of an inverse-6 crystal at a reduced density $\rho^* = 2.06$, significantly below the equilibrium bulk melting density, $\rho^* = 2.206$. This is a 225-particle system created by removing one particle from a 256-particle fcc crystal. The vacancy diffuses rapidly in this system, but there is no evidence of liquidlike disorder. This plot was generated from a 5000 time-step ($\Delta t^* = 0.005$) run. The lines connect the position of each particle at time intervals of 100 steps.

crystals we observed surrounding vacancies were truly stable, we constructed a process by which a translationally disordered region is introduced into a crystalline environment. More specifically, a region containing N_s solid lattice sites is replaced by a liquidlike droplet containing $N_s - n_{\text{vac}}$ particles. The details of the procedure are discussed below. In effect, this initializes the system on the “premelting” side of a possible free-energy barrier, if indeed such a barrier to premelting exists. However, we found that any such liquidlike region containing up to four vacancies spontaneously ordered under all conditions where the bulk solid is thermodynamically stable, and even in a metastable (superheated or superexpanded) solid.

Equilibration of a liquidlike droplet inside a crystal is achieved by dividing the periodic simulation cell into two regions, and the particles into two sets. The “free” region contains the vacancies, premelted droplet (if one exists), and a portion of the surrounding solid. The rest of the simulation cell is called the “single-occupancy” region. The particles of the single-occupancy region are not allowed to stray more than halfway from their perfect lattice positions to the perfect lattice positions of neighboring particles, i.e., they are confined to Wigner-Seitz cells of the fcc lattice. This arrangement is shown schematically in Fig. 3. At high density, the single-occupancy constraints (i.e., one particle per Wigner-Seitz cell) has negligible effect on the crystal. In fact, a single-occupancy system was used to construct a reversible path

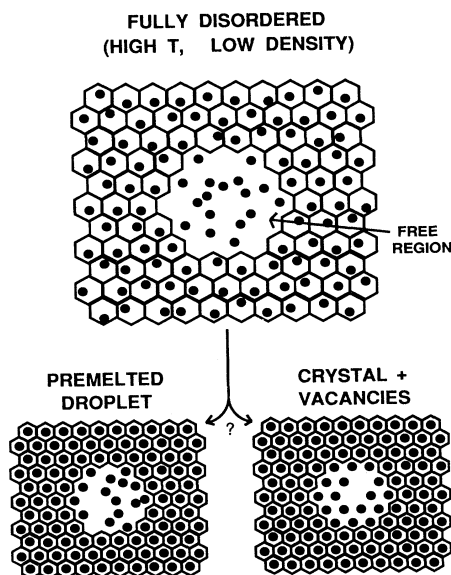


FIG. 3. Schematic representation of the procedure by which a liquidlike droplet is embedded into a solid. At low density (upper panel) the particles of the free region are completely disordered. There are no long-range correlations among the particles surrounding the free region which are artificially confined to Wigner-Seitz cells about each lattice point. At high density (lower panels) the single-occupancy particles order at a density lower than the bulk freezing density. The particles of the free region are not subject to any ordering constraints other than by interaction with the single-occupancy region. Because the figure is schematic and drawn for a small number of particles, it does not do justice to the actual numerical simulation in one important respect: The number of particles in the free region is actually much larger than the number we expect to be involved in premelting. This is necessary to minimize any artifacts arising from the single-occupancy constraints. The free region of our largest simulations, reported in Figs. 4 and 5, contained 438 particles.

to the crystal in the original determination of the coexistence parameters of the inverse-6 soft spheres.³¹ The Wigner-Seitz constraints are a sum of discontinuous, one-body potentials applied to all particles of the single-occupancy region. We switched from molecular dynamics to Monte Carlo sampling for convenience in treating the nondifferentiable cell constraints.

In practice, the particles of the free region were identified as those within a certain distance, R_{free} from the center of the simulation cell. The free region would hold N_{free} Wigner-Seitz cells in a perfect crystal, but contains $N_{\text{free}} - n_{\text{vac}}$ particles in the defected solid. The rest of the simulation cell, the single-occupancy region, contains one particle per Wigner-Seitz cell. During the simulation, the particles of the free region are allowed to penetrate a small distance into the single-occupancy region. In our largest simulations of this type, R_{free} was 4.1 nearest-neighbor distances of a perfect crystal at the initial density of $\rho^* = \sim 1.5$. This gave $N_{\text{free}} = 438$ out of a

total system of 4000 particles. The free particles were allowed to stray 4.5 nearest-neighbor distances from the midpoint of the cell at the initial density. As the system is compressed, the range of motion of the free particles was not changed (i.e., was not scaled with density), allowing the free particles, in principle, to penetrate further into the single-occupancy region. This constraint only had an effect on the system during equilibration at low densities, where the free particles would, on rare occasions, become trapped in the single-occupancy region. At higher densities, the crystal lattice prevented deep

penetration into the single-occupancy region. Using Eq. (4) and the known coexistence parameters for the inverse-6 model, an upper limit to the number of particles involved in a premelted droplet would be $\sim 77.8n_{\text{vac}}$. The 438 particle-free region was larger than this estimate for all values of n_{vac} studied, overwhelmingly so for $n_{\text{vac}}=1$ or 2.

A series of simulations is begun at low density. Initially there are no long-range correlations among the particles of the single-occupancy region. As the system is compressed, the particles of the single-occupancy region

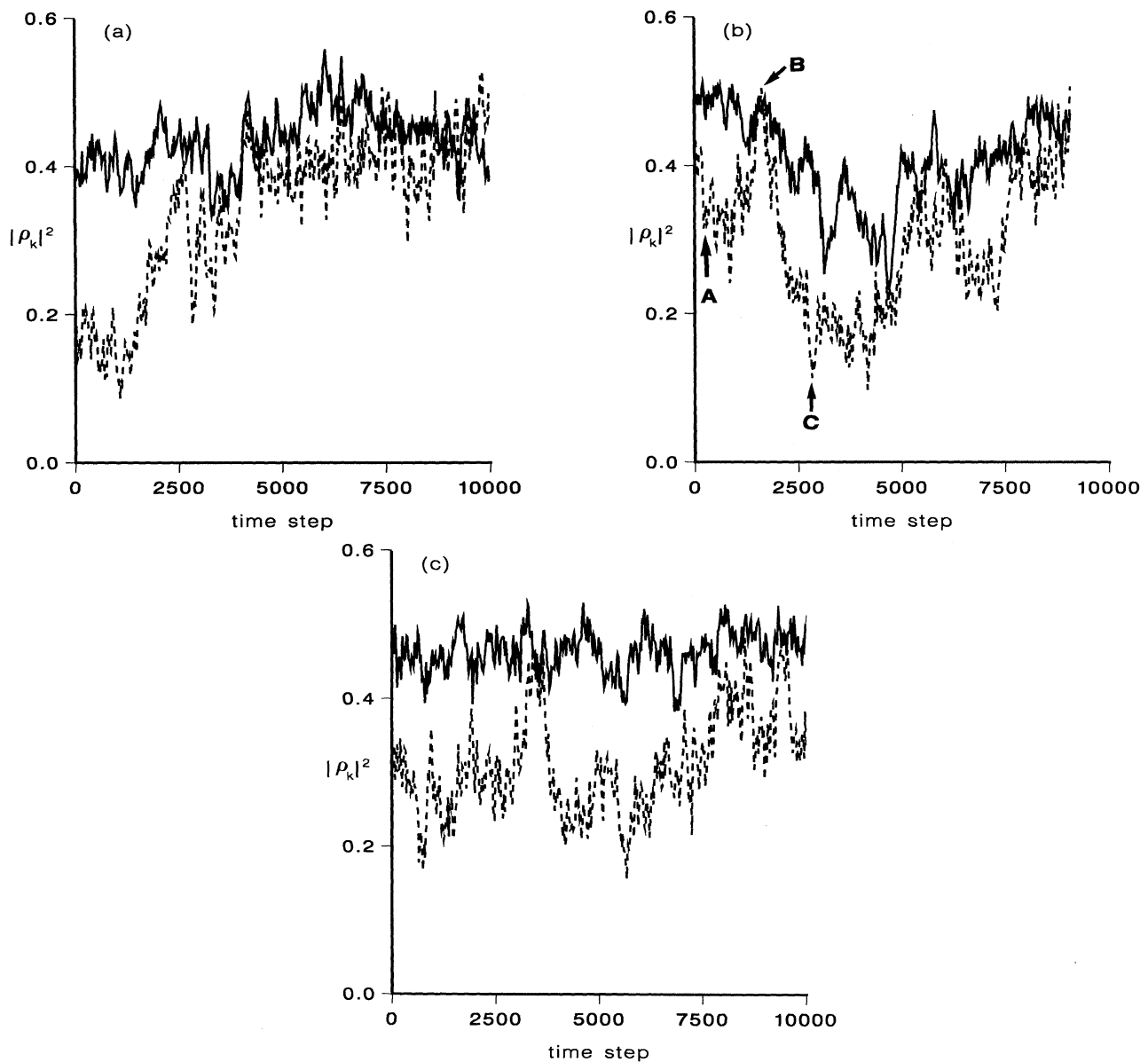


FIG. 4. The solid and dashed lines are the order parameter [Eq. (8)] of the single-occupancy and free regions, respectively, as a function of time (time step $\Delta t^*=0.005$). If free of vacancies, the system holds 4000 particles, 438 allocated to the free region. (See Sec. III in the text.) In each case the single-occupancy region was already ordered and the free region was at the point of spontaneously ordering at a density below the bulk freezing point: (a) $\rho^*=2.05$, $n_{\text{vac}}=0$; (b) $\rho^*=2.05$, $n_{\text{vac}}=2$; (c) $\rho^*=2.1$, $n_{\text{vac}}=4$. (b) is especially interesting because the system was captured at the point where the free region was exhibiting a reversible equilibrium between solidlike and liquidlike order. Particle configurations associated with points *A*, *B*, and *C* in (b) are shown in Fig. 5.

undergo a phase transition in which they acquire long-range positional order. This transition occurs at a density below the bulk freezing transition, in our simulations, in the range $\rho^* \approx 2.05$ – 2.10 . At this point, we have constructed an artificially stabilized solid (at a density where the unconstrained system would be fluid), and a liquid droplet in the free region. Further compression equilibrates an initially disordered droplet within a crystal.

The single-occupancy–free-region construction has permitted us to concentrate all n_{vac} vacancies within the free region of the simulation cell. The initially disordered free region can be equilibrated with artificially stabilized single-occupancy solid before the density is increased to the bulk freezing point. Once the crystal is brought to densities at which the solid is stable, then events in which particles sample the Wigner-Seitz cell boundaries are rare and the single-occupancy constraints have negligible effect. In addition, the free particles no longer explore far beyond the boundary of the single-occupancy region. One may anticipate that the crystal surrounding a premelted droplet might be relaxed from their perfect lattice positions. For our construction to be valid, the free region must contain any highly relaxed crystalline particles surrounding the disordered region, as well as a premelted droplet, should it form. We performed a series of runs with increasingly large free regions. Since we desired maximum separation between the closest boundaries of free regions of neighboring periodic simulation cells (typically 4–6 nearest-neighbor distances of a perfect lattice), the total number of particles in the simulation increased with the size of the free region. To economize on the total number of particles we needed to simulate, a truncated octahedron geometry was employed for the simulation cell. Compared to a cubic simulation cell, the truncated octahedron requires roughly half as many particles to separate two periodically replicated free regions by the same distance.

Figure 4 shows typical behavior upon compression of the free-region–single-occupancy system. The free region invariably ordered almost immediately after the single-occupancy region underwent its ordering phase transition. Both events occurred at densities significantly below the bulk freezing transition. Therefore, we conclude that premelted droplets will not be associated with vacancies, or polyvacancies up to $n_{\text{vac}} = 4$, in the inverse-6 soft-sphere model. On the basis of qualitative arguments presented in Sec. II, we believe that smaller inverse- n exponents are most conducive to vacancy-induced premelting. Therefore, we have obtained strong evidence that vacancy-induced premelting will not occur for the entire family of inverse power potentials with exponents greater than 6. Even relatively soft atomic cores are typically parametrized with exponents greater than 6. Hence, it is doubtful that vacancy-induced premelting is a general feature of the packing of particles in a defected crystalline lattice.

There is one feature of the free-region–single-occupancy system that deserves special notice, even though the effect occurred below the bulk melting density. Figure 4(b) shows the magnitude of the crystalline order parameter as a function of time for the free region at

$\rho^* = 2.05$. This density is below the bulk freezing density, so large-range translational order of the particles outside the free region is entirely due to the single-occupancy constraints. Figure 4(b) exhibits a reversible equilibrium between solidlike and liquidlike order in the free region.

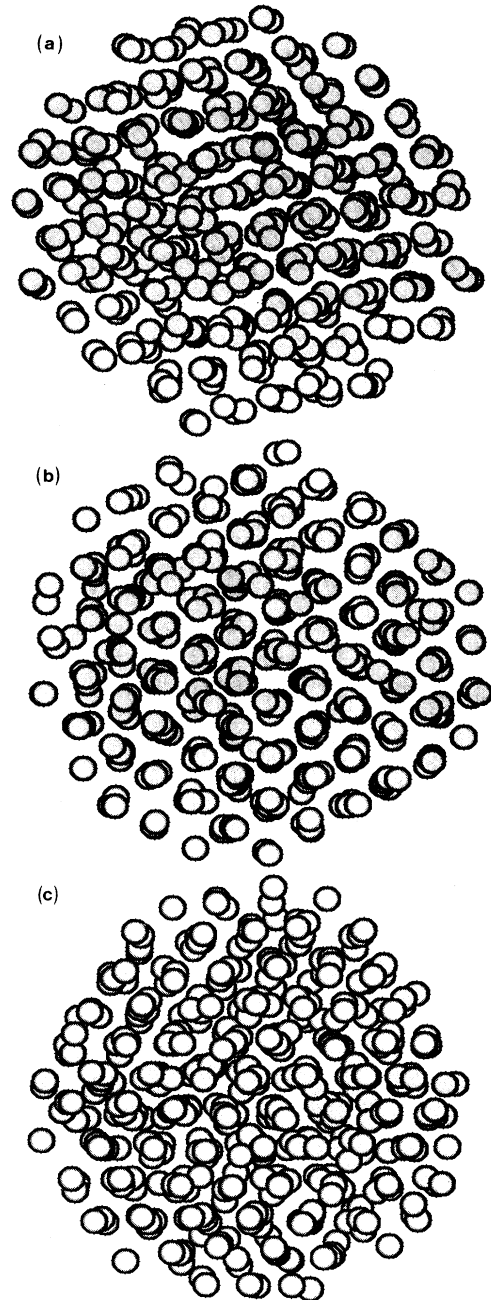


FIG. 5. Particle configurations of the free region ($\rho^* = 2.05$, $n_{\text{vac}} = 2$) during at three instants during the run shown in Fig. 4(b). (a)–(c) of this figure correspond to the points marked A, B, and C in Fig. 4(b). The degree of translational order leading to the order-parameter fluctuations shown in Fig. 4(b) is best visualized by looking along lattice planes near the center of the cluster. (The edges of the free region are always ordered to some extent by close interaction with the single-occupancy region.) (b) is most strongly ordered. (a) and (c) are almost liquidlike near the center.

At several points the order parameter of the free region (dashed line) is nearly equal to that of the surrounding single-occupancy region. At other times, there is significant gap between the degree of translational order in the free and single-occupancy regions. At intervals indicated by arrows in Fig. 4(b), three-dimensional views of the free regions were generated. Shown in Fig. 5, these views clearly show that the system becomes trapped in either solidlike or liquidlike conformations for appreciable numbers of Monte Carlo steps. Transitions between solidlike and liquidlike conformations are relatively rare events. This behavior is explained by the existence of two free-energy minima corresponding to solid and fluid free regions separated by a free-energy barrier.

Even though the behavior shown in Figs. 4(b) and 5 is entirely based on the presence of the single-occupancy constraints, it does point to interesting ramifications should point-defect premelting be found in other systems. Let us suppose that both equilibrium (i.e., point) and nonequilibrium (e.g., grain-boundary) defect premelting, as well as surface premelting, are governed by a Landau-Ginzburg-type free-energy function of an order parameter. The free energy *per particle* would have a characteristic double-well structure, and the well corresponding to disorder near the defect or surface would become the lowest free-energy minimum when the system entered the premelting region of the thermodynamic plane. For surface or grain-boundary premelting, the total free-energy difference between ordered and disordered systems scales as the free-energy difference per surface particle or per surface area, times the amount of surface ($\propto V^{2/3}$). The free-energy difference is the difference between minima of the Landau-Ginzburg free-energy function. Therefore, the *total* free-energy difference between ordered and premelted configurations, as well as the free-energy barrier between the two configurations, are both infinite in the thermodynamic limit for nonequilibrium defects. This is clearly not the case for premelting near isolated point defects. There should be a statistical ensemble of ordered and premelted point defects, the relative populations determined by the free-energy difference between the two configurations, finite even in the thermodynamic limit.

When the free-energy barrier between ordered and premelted point defects is not prohibitively large, then the crystal surrounding the defect should interconvert between the two configurations, much like dynamic equilibrium between two chemical isomers. This is precisely what is observed in Fig. 5, albeit for a point defect in an artificially stabilized crystal. However, if point-defect premelting is found to exist in other systems, we anticipate that a dynamic equilibrium between ordered and premelted configurations will also be possible. The behavior of point defects in this regard is entirely analogous to that of small van der Waals clusters, for which dynamic equilibrium between solid and liquid forms is observed in molecular-dynamics and Monte Carlo simulations.⁴¹⁻⁴³ The dynamic equilibrium effect depends on the details of the free-energy surface of the finite-sized system, and it is observed for some cluster sizes but not others. The situation should be analogous for point-defect premelting.

IV. STUDIES OF AN IMPURITY IN A SOFT-SPHERE CRYSTAL

XAFS and Mössbauer experiments probe the space-time correlation function of the impurity. We searched for abrupt changes in the behavior of an impurity in the r^{-6} model system as the solid phase approaches the melting point. Indeed, for relatively large size mismatch between impurity and bulk particles, we did detect a rapid increase in the formation of interstitial-vacancy ($I-V$) pairs above a temperature threshold. At still higher temperatures or lower densities, the closely bound $I-V$ pairs dissociated into independently diffusing interstitials and vacancies. It is not clear whether similar events lie behind experimental observations.^{1,2} If so, the experiments are explained by the onset of defect formation. There is no particular reason to eschew the traditional language of point defects and label formation of $I-V$ pairs as "premelting," other than the fact that defects by definition represent a relaxation of crystalline order and bring the system closer to melting.

What we call an impurity in our model is a particle (particle number 1, say) that interacts with any remaining particle j according to the potential,

$$v(\mathbf{r}_1 - \mathbf{r}_j) = \left[\frac{\frac{1}{2}(\sigma_{\text{imp}} + 1)}{|\mathbf{r}_1 - \mathbf{r}_j|} \right]^6. \quad (9)$$

We investigated impurities with diameters $\sigma_{\text{imp}} = 0.6, 0.8, 0.9$, and (by studying the "pure" bulk) 1, tracking the mean-squared displacement of the impurity from its perfect lattice site as a function of density, or equivalently temperature for an inverse-6 model. The purpose was to detect any abrupt change in the spatial distribution of the impurity which would signal premelting. Actually, no such change in the mean-squared displacement was observed until $I-V$ pairs were generated at $\sigma_{\text{imp}} = 0.6$. Until this point, the mean-squared impurity displacement as a function of density and impurity diameter could be fit by a simple analytical form with a minimum of free parameters. Because $I-V$ pair formation was a rare event, we collected information on the energetics of these processes, using concepts of activated rate processes to make inferences about temporal behavior. Also, evidence for the efficiency of impurity diffusion as interstitials is reported.

A. Spatial distribution of impurities

The intensity of the Mössbauer resonance line is dominated by the Debye-Waller factor, and therefore by the mean-squared displacement of Mössbauer-active nuclei. Mean-squared displacements are also estimated in XAFS experiments. Therefore, we primarily use the mean-squared displacement of impurity particles to track the local order near the impurity. We also monitored other aspects of the impurity particle distribution functions through trajectory plots, but, as mentioned before, found nothing anomalous until interstitial-vacancy pairs formed for a small impurity particle diameter. $I-V$ pair formation is discussed in Sec. IV B.

Figure 6 shows the mean-squared displacement of the impurity particle $\langle r_1^2 \rangle$ for $\sigma_{\text{imp}}=1$, the bulk system, and for $\sigma_{\text{imp}}=0.9, 0.8$, and 0.6 . $\langle r_1^2 \rangle$ is measured from the perfect lattice position of a substitutional impurity. The data are plotted against the reduced temperature T^* so that the low-temperature harmonic limit is made apparent as the linear portion of the graph. [For inverse-6 soft spheres in three dimensions, $T^*=(\rho^*)^{-2}$.] When $\sigma_{\text{imp}}=1$, $\langle r_1^2 \rangle$ could be determined with less than a percent error because the data from all particles in a bulk r^{-6} crystal were averaged. Within experimental error, the mean-squared displacement in the bulk crystal was fit by a quadratic in the reduced temperature:

$$\langle r_1^2 \rangle_{\sigma_{\text{imp}}=1} \approx 0.036000T^* + 0.093147T^{*2}. \quad (10)$$

The error bars for $\langle r_1^2 \rangle$ when $\sigma_{\text{imp}} < 1$ are considerably larger since this is derived from the behavior for just one particle. Within statistical error, the data for $\sigma_{\text{imp}}=0.9, 0.8$, and 0.6 could be fit by adding just three more fitting parameters. By standard thermodynamic perturbation theory about the bulk crystal as a reference system, the difference between $\langle r_1^2 \rangle$ for the impurity and $\langle r_1^2 \rangle$ for the bulk can be shown to be a function of T^* and y , where

$$y \equiv [\frac{1}{2}(\sigma_{\text{imp}} + 1)]^6 - 1. \quad (11)$$

The parameter y arises from the difference between the potential of the crystal containing an impurity and the bulk potential. The curves through the data in Fig. 6

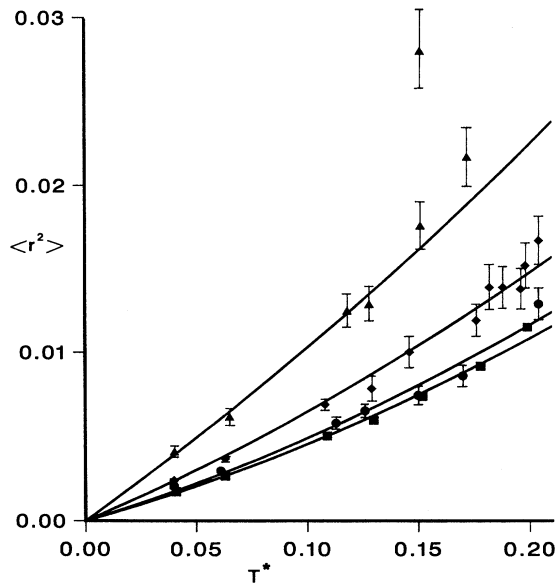


FIG. 6. Mean-squared displacement as a function of T^* for $\sigma_{\text{imp}}=1$ (■), 0.9 (●), 0.8 (◆), and 0.6 (▲). Error bars indicate an uncertainty of one standard deviation. The solid lines are the polynomial fit given in Eq. (10)–(12). Interstitial-vacancy pairs were observed in the runs at $\sigma_{\text{imp}}=0.6$ where the measured $\langle r_1^2 \rangle$ lies far above the polynomial fit. The bulk inverse-6 crystal melts at $T^*=0.205$.

have the analytic form

$$\langle r_1^2 \rangle_{\sigma_{\text{imp}}} = \langle r_1^2 \rangle_{\sigma_{\text{imp}}=1} + 0.023233T^*y + 0.13681T^*y^2 - 0.0022089T^{*2}y. \quad (12)$$

Over most of the parameter range in Fig. 6, the behavior of $\langle r_1^2 \rangle$ as a function of T^* and σ_{imp} is described by a low-order polynomial fit. If there is a sudden change in the behavior of an impurity of diameter $\sigma_{\text{imp}}=0.8$ or 0.9 as the bulk melting point is approached, it is not reflected in the smooth behavior of $\langle r_1^2 \rangle$. We regard this as evidence that nothing except the increased free volume available to an impurity with small diameter is controlling $\langle r_1^2 \rangle$. There is a clear break in the behavior of $\langle r_1^2 \rangle$ above $T^* \sim 0.15$ for $\sigma_{\text{imp}}=0.6$. Indeed, we can trace this to the onset of I - V pair formation, and not to premelting near the impurity.

B. Interstitial-vacancy pair formation

Impurities of diameter $\sigma_{\text{imp}}=0.6$ were observed to fluctuate between substitutional impurities and interstitial-vacancy pairs. A typical trajectory at $\rho^*=2.6$ is shown in Fig. 7. The impurity particle (solid line) is seen to dwell in an octahedral interstitial site for ~ 600 time steps. During this time a vacancy is created at the original substitutional site. The vacancy diffuses (dashed line) while the impurity lingers at an interstitial site. By the end of the 3000 time-step segment, the interstitial im-

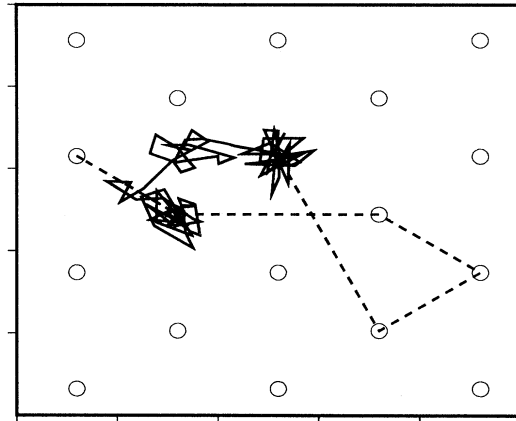


FIG. 7. The solid and dashed lines are the trajectories of an impurity and vacancy, respectively, at $\rho^*=2.6$, $\sigma_{\text{imp}}=0.6$. During this 3000 time-step run the impurity begins as a substitutional defect, oscillating near one of the perfect lattice positions of the fcc lattice indicated by open circles. The impurity then jumps to an octahedral interstitial site. For this viewing direction, $(0,1,-1)$, the octahedral sites lie midway between horizontal or vertical pairs of neighboring open circles. Hopping to an interstitial site creates a vacancy which eventually diffuses away from the original substitutional site. Finally, the interstitial and vacancy recombine to form a substitutional impurity at a different location from the original substitutional. The straight line segments connect positions which are output every 30 time steps ($\Delta t^*=0.005$). The position of a vacancy is calculated by associating each bulk particle with the closest perfect lattice position. The vacancy position is then assigned to the perfect lattice site without an associated particle.

purity and vacancy have recombined to form a substitutional impurity at a new lattice site. The trajectories of the particles near the impurity and vacancy have been monitored and no change in their spatial distribution is discernable. We first observed the onset of $I-V$ pair formation at $\rho^*=2.6$, $\sigma_{\text{imp}}=0.6$, but it is too rare at this density to permit estimation of its frequency. Our failure to observe $I-V$ pair formation at lower temperatures or densities and larger σ_{imp} is due to practical limits on simulation times.

Having identified $I-V$ pair formation as the first observed break from the smooth increase of vibrational amplitudes captured in Eq. (12), it is natural to ask whether these events could produce the features in Mössbauer spectra attributed to premelting. We present evidence below that suggests that the diffusion constant of an interstitial impurity is much greater than the substitutional impurity. Whether sudden intermittent changes in the diffusion constant of a Mössbauer active particle can explain the experimental spectra will be considered in a separate work.⁴⁴

Once the $I-V$ pair is formed, it is possible for the interstitial and vacancy to dissociate from each other and diffuse independently. Despite the impracticality of attempting to precisely determine the rates of these rare events by direct simulation, we can make several inferences from our studies. We have monitored independently diffusing interstitials and vacancies. This characterizes the system long after the substitutional impurity has

formed an $I-V$ pair and the interstitial and vacancy have separated. From data such as $|\mathbf{r}_i(t) - \mathbf{r}_i(0)|^2$ ($\sigma_{\text{imp}}=0.6$, $\rho^*=2.6$) for the independent interstitial or vacancy (Fig. 8), it appears that the vacancy diffusion rate is somewhat larger than the interstitial diffusion rate. Both far exceed the diffusion rate for a substitutional impurity. Similar plots at other densities reveal identical trends.

The potential-energy surface of the N -body system contains one deep minimum corresponding to a zero-temperature perfect crystal, and many other minima that correspond to defected configurations. By locating the potential minima that are associated with $I-V$ pairs, we can further characterize the defect formation process. Rapidly quenching defected configurations to zero temperature brings the system to a unique potential minimum associated with that configuration. This type of analysis has been developed by Stillinger and Weber, who speak of these potential minima as "inherent structures."⁴⁵ Weber and Stillinger have quenched configurations from a molecular-dynamics simulation of a bcc solid, finding vacancy, split-interstitial pairs to be the dominant defect mechanism as melting is approached.⁴⁶

Rapidly quenches of $I-V$ pair configurations, such as the one shown in Fig. 7, at various initial densities or temperatures consistently yielded an octahedral interstitial plus a vacancy. The precise value of this minimum depends on the location of the vacancy in relation to the interstitial. The value of several potential minima associated with $I-V$ pairs is given in Fig. 9. In units of kT , the quenched $I-V$ configurations lie $(3.1-3.3)\rho^{*2}$ above the

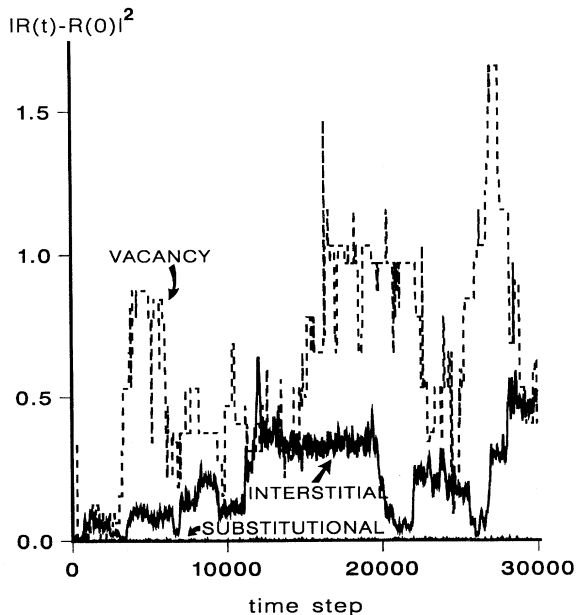


FIG. 8. The diffusive motion of a vacancy (dashed line), interstitial (solid line), and substitutional impurity (solid line barely visible above the bottom axis) is tracked by plotting the square of the distances traveled as a function of time ($\rho^*=2.6$, $\sigma_{\text{imp}}=0.6$, $\Delta t^*=0.005$). The position of a vacancy was calculated in the same manner described in the caption of Fig. 7. The vacancy and interstitial clearly diffuse far more rapidly than a substitutional impurity. The vacancy and interstitial plots show infrequent hops followed by many oscillations about a locally stable configuration.

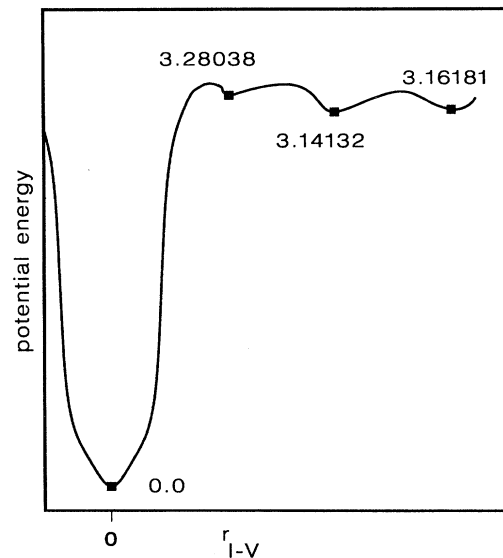


FIG. 9. Potential-energy minima were located for a 500-particle system containing a single impurity, $\sigma_{\text{imp}}=0.6$. Energies in units of kT are obtained from the numbers given above by multiplying by ρ^{*2} or, equivalently, by dividing by T^* . The energy of a fully relaxed substitutional impurity was taken as the zero of potential energy. The three local minima are interstitial-vacancy pairs with different distances between impurity and vacancy, as indicated schematically by the abscissa. The surface connecting the potential minima is also schematic, drawn to qualitatively reflect the diffusion data presented in Sec. IV.

substitutional impurity. For comparison, this energy difference would be $5.02\rho^{*2}$ without relaxation about the defects. The formation energy of an $I-V$ pair is quite large compared to kT , even near melting. To estimate the $I-V$ pair concentration, the entropy of formation and defect softening must also be considered.

Determining the potential barriers along minimum-energy paths connecting these low-energy configurations is a much more difficult exercise than finding the minima. The potential shown in Fig. 9 connecting potential minima is a sketch based on evidence described so far. Since formation of $I-V$ pairs is far less likely than diffusion of the separated vacancy and interstitial, the barrier from the substitutional impurity to the nearest $I-V$ pair potential minimum is drawn to be larger than the barrier between successive $I-V$ pair potential minima. Therefore, the motion of the impurity in Fig. 7 can be understood as vibrations about the local potential minimum corresponding to the $I-V$ pair, preceded and followed by activated barrier crossings to and from the deeper potential well that corresponds to the substitutional impurity configuration.

V. DISCUSSION OF RESULTS

From the data collected on vacancies and impurities in soft-sphere systems, the following picture of point-defect behavior near melting emerges. The ordering field of the surrounding crystal is sufficiently strong to prevent premelting near vacancies and polyvacancies up to tetra-vacancies. No unusual behavior other than larger vibrational amplitudes was observed for modest size mismatch between impurity and bulk particles. When $\sigma_{\text{imp}}=0.6$, we observed the onset of interstitial-vacancy pair formation when the density was 18% greater than the bulk melting density. As the density decreased, $I-V$ pairs dissociated into freely diffusing interstitials and vacancies. Although it is impractical to gather statistics on these rare events by direct simulation, we can make several inferences. The barrier to $I-V$ pair formation is significantly larger than the barrier to diffusion for an isolated interstitial. Therefore, the interstitial diffuses rapidly once it breaks free of the vacancy.

Based on the evidence presented in Sec. IV, we speculate that the behavior of a small impurity in the r^{-6} lat-

tice may be classified under three regimes: (1) $I-V$ pair formation is rare, (2) $I-V$ pair formation is frequent, but the interstitial and vacancy remain closely bound to each other and eventually recombine, and (3) there exist equilibrium populations of substitutional impurities and freely diffusing interstitials and vacancies. [In our opinion the data is certainly suggestive of regimes (1) and (3), but it is not clear that regime (2) persists over a significant range of density or temperature.] Simple impurity diffusion is ruled out as an explanation of the anomalous Mössbauer intensity of tin impurities in a lead host near melting because the lines are not broadened.² The line shape in regime (3) depends upon the fraction of time the impurity spends as a rapidly diffusing interstitial and a relatively immobile substitutional.⁴⁴ Except at zero Mössbauer photon wave vector, the linewidth is *not* an average of widths characteristic of the interstitial and substitutional weighted by the populations of the two defect states.⁴⁴

The limitations of our calculations must be considered before applying our results to explain experimental results. Different interaction potentials may lead to qualitatively different premelting behavior. Lattice structures which are not close packed may also behave differently than the fcc crystal investigated here. (For example, Weber and Stillinger found split interstitials in their simulations of a bcc crystal.⁴⁶) We took great pains to eliminate time length and system size of our simulations as explanations of our failure to observe point-defect premelting. Nevertheless, all numerical simulations are subject to practical limitations. Since the mechanism of equilibrium, bulk melting (if it exists) remains poorly understood, our hope is that the results presented here will stimulate theoretical investigations of other models, and experiments that will more precisely characterize the local order near point defects.

ACKNOWLEDGMENTS

The calculations reported here were made possible by a grant from the Ohio Supercomputer Center. This research was supported by the Camille and Henry Dreyfus Foundation, and by the Donors of the Petroleum Research Fund, administered by the American Chemical Society. One of us (S.J.S.) thanks Edward Stern for a helpful conversation.

¹E. A. Stern and K. Zhang, Phys. Rev. Lett. **60**, 1872 (1988).

²H. Shechter, E. A. Stern, Y. Yacoby, R. Brenner, and Z. Zhang, Phys. Rev. Lett. **61**, 1400 (1988).

³M. Pokorny and G. Grimvall, J. Phys. F **14**, 931 (1984).

⁴J. W. M. Frenken and J. F. van der Veen, Phys. Rev. Lett. **54**, 134 (1985).

⁵J. Q. Broughton and G. H. Gilmer, J. Phys. Chem. **91**, 6347 (1987).

⁶F. J. Bartis, Philos. Mag. A **52**, L33 (1985).

⁷F. J. Bartis, Philos. Mag. Lett. **60**, 17 (1989).

⁸A. R. Ubbelohde, *Melting and Crystal Structure* (Clarendon, Oxford, 1965).

⁹R. M. J. Cotterill, Phys. Bull. **32**, 285 (1981).

¹⁰W. Hayes, Contemp. Phys. **27**, 519 (1986).

¹¹N. H. Nachtrieb and G. S. Handler, Acta. Metall. **2**, 797 (1954).

¹²F. J. Bartis, Nature **268**, 427 (1977); **276**, 849 (1978).

¹³J. L. Tallon, Nature **276**, 849 (1978).

¹⁴R. W. Cahn, Nature **273**, 491 (1978).

¹⁵R. W. Cahn, Nature **323**, 668 (1986).

¹⁶H. Saka, Y. Nishikawa, and T. Imura, Philos. Mag. **57**, 895 (1988).

¹⁷H. Reiss, *Methods of Thermodynamics* (Blaisdell, New York, 1965).

¹⁸J. Q. Broughton and G. H. Gilmer, J. Chem. Phys. **79**, 5095 (1983).

- ¹⁹J. Q. Broughton and G. H. Gilmer, *Phys. Rev. Lett.* **56**, 2692 (1986).
- ²⁰G. Devaud and R. H. Willens, *Phys. Rev. Lett.* **57**, 2683 (1986).
- ²¹D.-M. Zhu and J. G. Dash, *Phys. Rev. Lett.* **60**, 432 (1988).
- ²²P. von Blackenhagen and W. Schommers, *Static and Dynamic Properties of Liquids* (Springer-Verlag, Heidelberg, 1989), p. 58.
- ²³F. F. Abraham and J. Q. Broughton, *Phys. Rev. Lett.* **56**, 734 (1986).
- ²⁴P. Stoltze, J. K. Norskov, and U. Landman, *Phys. Rev. Lett.* **61**, 440 (1988).
- ²⁵S. R. Phillpot, J. F. Lutsko, D. Wolf, and S. Yip, *Phys. Rev. B* **40**, 2831 (1989).
- ²⁶J. F. Lutsko, D. Wolf, S. R. Phillpot, and S. Yip, *Phys. Rev. B* **40**, 2841 (1989).
- ²⁷R. M. J. Cotterill, E. J. Jensen, and W. D. Kristensen, *Phys. Rev. Lett.* **44A**, 127 (1973).
- ²⁸R. M. J. Cotterill, E. J. Jensen, and W. D. Kristensen, *Philos. Mag.* **30**, 229 (1974).
- ²⁹J. P. Hansen and I. R. McDonald, *Theory of Simple Liquids*, 2nd. ed. (Academic, New York, 1986).
- ³⁰W. G. Hoover, M. Ross, K. W. Johnson, D. Henderson, J. A. Barker, and B. C. Brown, *J. Chem. Phys.* **52**, 4931 (1970).
- ³¹W. G. Hoover, S. G. Gray, and K. W. Johnson, *J. Chem. Phys.* **55**, 1128 (1978).
- ³²W. G. Hoover, D. A. Young, and R. Grover, *J. Chem. Phys.* **56**, 2207 (1972).
- ³³J. D. Weeks, *Phys. Rev. B* **24**, 1530 (1981).
- ³⁴J. D. Weeks, D. Chandler, and H. C. Andersen, *J. Chem. Phys.* **54**, 5237 (1971); D. Chandler and J. D. Weeks, *Phys. Rev. Lett.* **25**, 149 (1970); J. D. Weeks, D. Chandler, and H. C. Andersen, *J. Chem. Phys.* **55**, 5422 (1971).
- ³⁵J. C. Langeberg, R. B. McLellan, and G. V. Bettoney, *J. Phys. Chem. Solids* **33**, 1391 (1972).
- ³⁶H. Kanzaki, *J. Phys. Chem. Solids* **2**, 24 (1957).
- ³⁷C. H. Bennett and B. J. Alder, *J. Phys. Chem. Solids* **32**, 2111 (1971).
- ³⁸D. R. Squire and W. G. Hoover, *J. Chem. Phys.* **50**, 701 (1969).
- ³⁹A. Meyer, M. Silbert, and W. H. Young, *Phys. Chem. Liq.* **10**, 279 (1981).
- ⁴⁰T. Grindley, *Phys. Chem. Liq.* **8**, 283 (1979).
- ⁴¹R. S. Berry, T. L. Beck, H. L. Davis, and J. Jelinek, *Adv. Chem. Phys.* **70**, 75 (1988).
- ⁴²R. S. Berry, in *Few-Body Systems and Multiparticle Dynamics*, Proceedings of the Symposia of the Topical Group on Few-Body Systems and Multiparticle Dynamics, AIP Conf. No. 162, edited by David A. Micha (AIP, New York, 1987), p. 261.
- ⁴³J. D. Honeycutt and H. C. Andersen, *J. Phys. Chem.* **91**, 4950 (1987).
- ⁴⁴S. J. Singer and C. H. Martin (unpublished).
- ⁴⁵F. H. Stillinger and T. A. Weber, *Science* **225**, 983 (1984).
- ⁴⁶T. A. Weber and F. H. Stillinger, *J. Chem. Phys.* **81**, 5095 (1984).